NUCL SCI TECH (2018) 29:161
https://doi.org/10.1007/s41365-018-0498-6

Influence of the shell effects on evaporation residue cross section of superheavy nuclei

D. Naderi[1] · S. A. Alavi[2]

Received: 16 March 2018 / Revised: 18 April 2018 / Accepted: 3 June 2018 / Published online: 28 September 2018

Abstract In order to study the influence of the shell effects on the formation and fission of superheavy elements, we applied multidimensional Langevin equations. The evaporation residue cross sections have been calculated for $3n$, $4n$, and $5n$ evaporation channels using three ($K=0$)- and four ($K \neq 0$)-dimensional Langevin equations. Calculations were done for ^{48}Ca + ^{238}U and ^{48}Ca + ^{244}Pu hot fusion reactions with $3n$, $4n$ evaporation channels and ^{70}Zn + ^{208}Pb, and ^{54}Cr + ^{209}Bi cold fusion reactions with $1n$ and $2n$ evaporation channels. The calculations were performed for $4n$ and $5n$ evaporation channels of the ^{26}Mg + ^{238}U reaction, as well. Our results show that with increasing dimension of Langevin equations the residue cross section increases, whereas the fission cross section decreases. The obtained results with four-dimensional Langevin and considering shell effects are in better agreement with experimental data in comparison with three- and four-dimensional Langevin equations without shell effects.

Keywords Superheavy · Langevin equations · Cross section

✉ S. A. Alavi
s.a.alavi@phys.usb.ac.ir

D. Naderi
d.naderi@razi.ac.ir

1 Department of Physics, Faculty of Basic Sciences, Razi University, Kermanshah 67149, Iran

2 Department of Physics, University of Sistan and Baluchestan, Zahedan 98135, Iran

1 Introduction

The superheavy elements production is one of the important problems and outstanding research objects of recent nuclear physics. Some experimental and theoretical research has been done to produce and investigate the synthesis mechanism of superheavy elements. Cold fusion and hot fusion are two main classes of the heavy-ion fusion reactions for synthesis of superheavy nuclei. The superheavy nuclei with $Z = 102$–118 have been produced by means of cold fusion reactions with the targets of ^{208}Pb and ^{209}Bi and ^{48}Ca-induced hot fusion reactions [1–5].

Various theoretical methods have been introduced for study of the superheavy nucleus production, such as the dynamical Langevin model [6–8], dinuclear system model [9–11], fluctuation dissipation model [12, 13], nuclear collectivization concept [14], macroscopic dynamical model [15], and multidimensional stochastic model [16]. In Ref. [17] the dynamical Langevin model has been used to estimate ^{58}Fe + ^{238}Pb cold fusion reaction cross sections. In a similar manner, this method (one-dimensional Langevin equation) has been used for ^{48}Ca + ^{238}U hot fusion reaction in Refs. [18, 19]. In order to determine the cold and hot fusion reaction cross sections, the dinuclear system was used in Refs. [20–23].

In this paper, we applied multidimensional Langevin equations to evaluate the formation of a superheavy nucleus. The main topics of this paper are the analysis of the influence of the orientation degree of freedom and shell effects on synthesis of superheavy nucleus. In Sect. 2 the theoretical calculations based on Langevin equations are given. The obtained results are given in Sect. 3. Finally, the summary and conclusion remarks are presented in Sect. 4.

2 Model

The fusion and fission processes are considered with the same approach. The Langevin equations for the shape parameters of the ions give the time evolution of the system in both stages. The random force term gives the stochastic features of the process. For easiness, the shape of the system is considered in terms of two spheres with radii R_1 and R_2 gently connected with hyperboloidal neck. Let r stands for the total length of the system, $s = r - 2(R_1 + R_2)$ for the surface separation between the two spheres, h is the radius of the neck, and $\alpha = [(R_1 - R_2)/(R_1 + R_2)]^2$ is the asymmetry variable. The coupled Langevin equations of motion in multidimensional collective space are written as [17, 24–26]

$$\begin{aligned}\frac{\mathrm{d}q_i}{\mathrm{d}t} &= \mu_{ij} p_j,\\ \frac{\mathrm{d}p_i}{\mathrm{d}t} &= -\frac{1}{2} p_j p_k \frac{\partial \mu_{jk}}{\partial q_i} - \frac{\partial V(q)}{\partial q_i} - \gamma_{ij}\mu_{jk}p_k + \theta_{ij}\xi_j(t),\end{aligned} \tag{1}$$

where $q_i = s, h, \alpha$ represent the collective coordinates, p_i gives conjugate momenta, and μ_{jk} denotes inverse matrix elements of the inertia tensor, m_{ij} [27, 28]. The strength θ_{ij} of the random force is given by $\theta_{ik}\theta_{kj} = T\gamma_{ij}$. T and γ_{ij} are the temperature and friction tensor, respectively [24].

The potential energy of the system is defined as [29]

$$\begin{aligned}V(q,I,K,T) =& V_{\mathrm{LD}}(q) + \frac{[I(I+1) - K^2]\hbar^2}{[0.8MR_0^2 J_\perp(q) + 8Ma^2]}\\ &+ \frac{K^2\hbar^2}{[0.8MR_0^2 J_\parallel(q) + 8Ma^2]} + V_{\mathrm{SH}}(q,T),\end{aligned} \tag{2}$$

where $V_{\mathrm{LD}}(q)$ is the potential energy based on the liquid-drop model. $R_0 = 1.2249A^{1/3}$. A and M are the mass number and mass of the compound nucleus, respectively. $a = 0.6$ fm. $J_\parallel(q)$and $J_\perp(q)$ are the rigid body moments of inertia of the nucleus with respect to the symmetry axis and an axis orthogonal to it, respectively. K is the projection of the total spin of the compound nucleus (I) to the symmetry axis. The temperature-dependent shell correction energy, V_{SH}, is given as

$$V_{\mathrm{SH}}(q,T) = [\Delta E_{\mathrm{Pair}}(q) + \Delta E_{\mathrm{Shell}}(q)]\Phi(T), \tag{3}$$

where $\Delta E_{\mathrm{Pair}}(q) = E_{\mathrm{Pair}} - \langle E_{\mathrm{Pair}}\rangle$ is the pairing correlation energy which is determined by using *BCS* approximation [30]. Here $\langle E_{\mathrm{Pair}}\rangle$ is the average of pairing energy at the ground state distortions. We can calculate the pairing correlation energy based on the method of Ref. [30]. Also $\Delta E_{\mathrm{Shell}}(q)$ is the shell correction energy based on the Strutinsky method which can be defined as [31–33]

$$\Delta E_{\mathrm{Shell}}(q) = \sum \epsilon_k - \int_{-\infty}^{\mu} e g(e)\mathrm{d}e, \tag{4}$$

ϵ_k, $g(e)$, μ are the energy, single particle density of states, and chemical potential, respectively. The temperature-dependent shell correction factor, $\Phi(T)$, in Eq. (3) is given as [34]

$$\Phi(T) = \exp\left(-\frac{aT^2}{E_{\mathrm{d}}}\right), \tag{5}$$

where $E_{\mathrm{d}} = 18.5$ MeV is the shell damping energy. a is the level density parameter [35]

$$\begin{aligned}a =& \left\{1 + \frac{V_{\mathrm{SH}}(T=0)}{E_{\mathrm{int}}}\left[1 - \exp\left(-\frac{E_{\mathrm{int}}}{E_{\mathrm{d}}}\right)\right]\right\}\\ &\times (a_1 A + a_2 A^{2/3} B_{\mathrm{s}}(q)),\end{aligned} \tag{6}$$

with $a_1 = 0.068$ MeV^{-1} and $a_2 = 0.213$ MeV^{-1} [35]. The alternative form of these parameters as $a_1 = 0.073$ MeV^{-1} and $a_2 = 0.095$ MeV^{-1} has been given by Ignatyuk [36]. The nuclear temperature can be calculated as

$$T = \sqrt{\frac{E_{\mathrm{int}}}{a}}. \tag{7}$$

The function $B_{\mathrm{s}}(q)$ is the dimensionless function of the surface energy in the liquid-drop model with a sharp surface [35]. The intrinsic excitation energy is calculated as,

$$E_{\mathrm{int}} = E_{\mathrm{c.m.}} + Q - V(q,I,K,T=0) - E_{\mathrm{Coll}}, \tag{8}$$

where the Q-value is the released energy of the reaction and E_{Coll} is the kinetic energy of the fusing system.

The variation of the orientation degree of freedom (K coordinate) is obtained as [37–39]

$$dK = -\frac{\gamma_K^2 I^2}{2}\frac{\partial V}{\partial K}dt + \gamma_K I\sqrt{\frac{Tdt}{2}}\xi(t). \tag{9}$$

Here the spins of projectile and target nuclei have been neglected and $I = l$. $\xi(t)$ is a random variable given as

$$\begin{aligned}&\langle \xi_i \rangle = 0,\\ &\langle \xi_i(t_1)\xi_j(t_2)\rangle = 2\delta_{ij}\delta(t_1 - t_2).\end{aligned} \tag{10}$$

The γ_K parameter controls the coupling between the orientation degree of freedom and heat bath [8, 38].

The evaporation residue cross section of a superheavy nucleus production is calculated as [40]

$$\begin{aligned}\sigma_{\mathrm{ER}} =& \frac{\pi\hbar^2}{2\mu E_{\mathrm{cm}}}\sum_{l=0}^{\infty}(2l+1)P_{\mathrm{cap}}(E_{\mathrm{cm}}, l)\\ &\times P_{\mathrm{fus}}(E_{\mathrm{cm}}, l)P_{\mathrm{kn}}(E_{\mathrm{cm}}, l).\end{aligned} \tag{11}$$

P_{cap} is the capture probability of the colliding nuclei. This factor can be calculated by means of the semiphenomenological barrier distribution function as [14, 40]

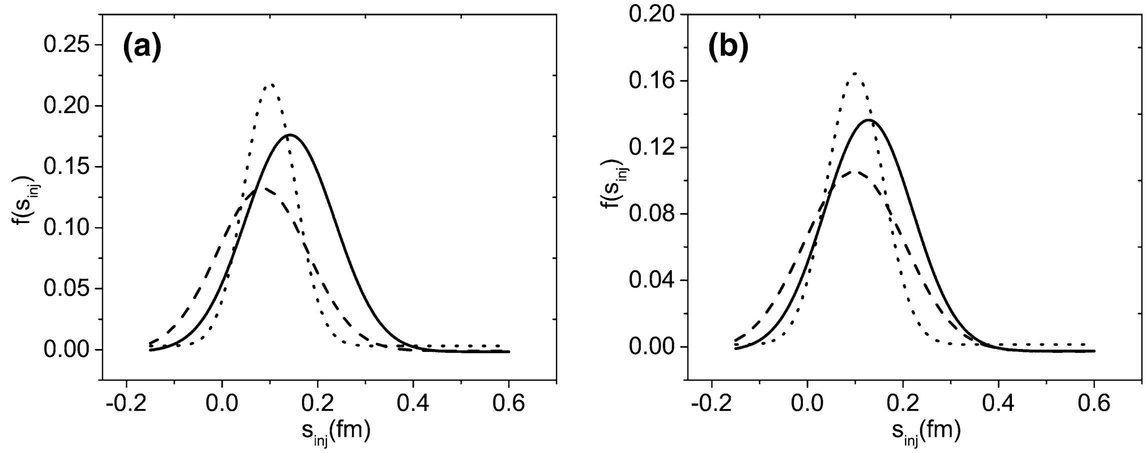

Fig. 1 Variations of the probability distributions of s_{inj} for **a** ^{48}Ca + ^{238}U reaction, **b** ^{48}Ca + ^{244}Pu reaction at $E_{\mathrm{cm}} = 200$ MeV. Dashed, solid, and dotted curves are the results based on three-dimensional Langevin equations without shell effects, four-dimensional Langevin equations without shell effects, and four-dimensional with shell effects, respectively

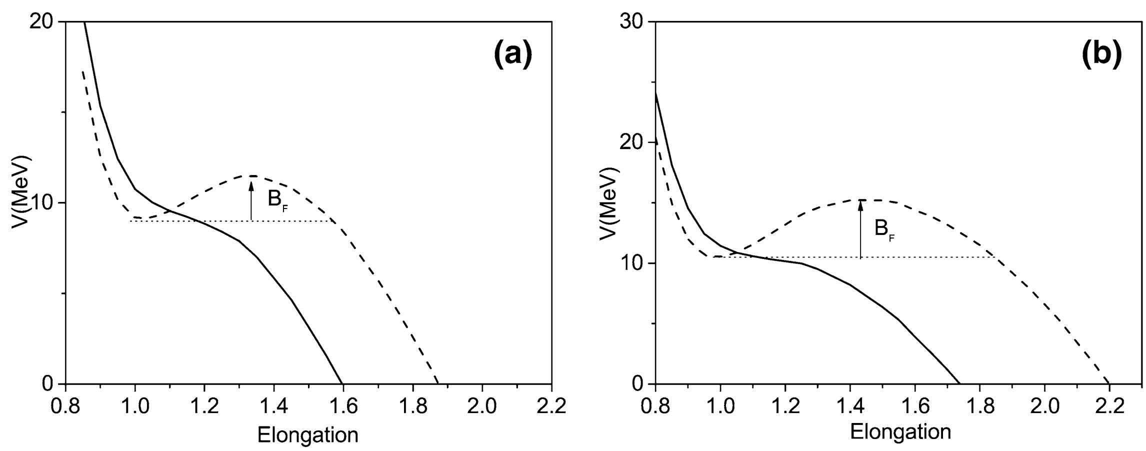

Fig. 2 Variations of the potential energy as a function of elongation for **a** ^{48}Ca + ^{238}U and **b** ^{28}Mg + ^{238}U reactions. Dashed and solid curves are the results for $I = 60, K = 60$ and $I = 60, K = 0$, respectively. B_{F} is the fission barrier

$$P_{\mathrm{cap}} = \int f(B) \frac{1}{1 + \exp\left(\frac{2\pi}{\hbar\omega_{\mathrm{B}}(l)}\left(B + \frac{\hbar^2}{2\mu R_{\mathrm{B}}^2} l(l+1) - E_{\mathrm{cm}}\right)\right)} \mathrm{d}B, \tag{12}$$

here $\hbar\omega_{\mathrm{B}}(l)$ is defined by the width of the parabolic barrier. $f(B)$ is the barrier distribution function [40].

The modified fusion by diffusion model [41, 42] for evaluating the compound nucleus formation probability, P_{fus}, is given as

$$P_{\mathrm{fus}}(E_{\mathrm{cm}}, l) = \frac{1}{2} \int \mathrm{erfc}\left(\sqrt{\mathrm{B}(s_{\mathrm{inj}}, \mathrm{l})/\mathrm{T}}\right) \times f(s_{\mathrm{inj}}) \mathrm{d}s_{\mathrm{inj}}, \tag{13}$$

where s_{inj} is the distance between the surfaces of two approaching nuclei where injection into an asymmetric fission valley takes place and $f(s_{\mathrm{inj}})$ is the probability distributions of s_{inj}. The dynamic equations were solved step by step and obtained the probability distribution of s_{inj}.

The survival probability is given as [7, 40]

$$\begin{aligned} P_{\mathrm{kn}}(E_0^*, l_0) = & \left[\frac{\Gamma_{\mathrm{n}}}{\Gamma_{\mathrm{tot}}}(E_0^*, l_0)\right] \int_0^{E_0^* - Sn(1)} \frac{\Gamma_{\mathrm{n}}}{\Gamma_{\mathrm{tot}}}(E_1^*, l_1) \\ & \times P_{\mathrm{n}}(E_0^*, e_1)\mathrm{d}e_1 \\ & \times \int_0^{E_1^* - Sn(2)} \frac{\Gamma_{\mathrm{n}}}{\Gamma_{\mathrm{tot}}}(E_2^*, e_2) P_{\mathrm{n}}(E_1^*, e_2)\mathrm{d}e_2 \ldots \\ & \times \int_{K_{\mathrm{th}}}^{E_{k-1}^* - Sn(k)} P_{\mathrm{n}}(E_{k-1}^*, e_k)\mathrm{d}e_k, \end{aligned} \tag{14}$$

here $\Gamma_{\mathrm{tot}} \approx \Gamma_{\mathrm{n}} + \Gamma_{\mathrm{fis}}$ is the total decay width. The details of the calculation of the P_{cap}, P_{fus}, and P_{kn} have been represented in Ref. [8]. The survival probability to fission strongly depends on the fission barrier, B_{f}, and how this

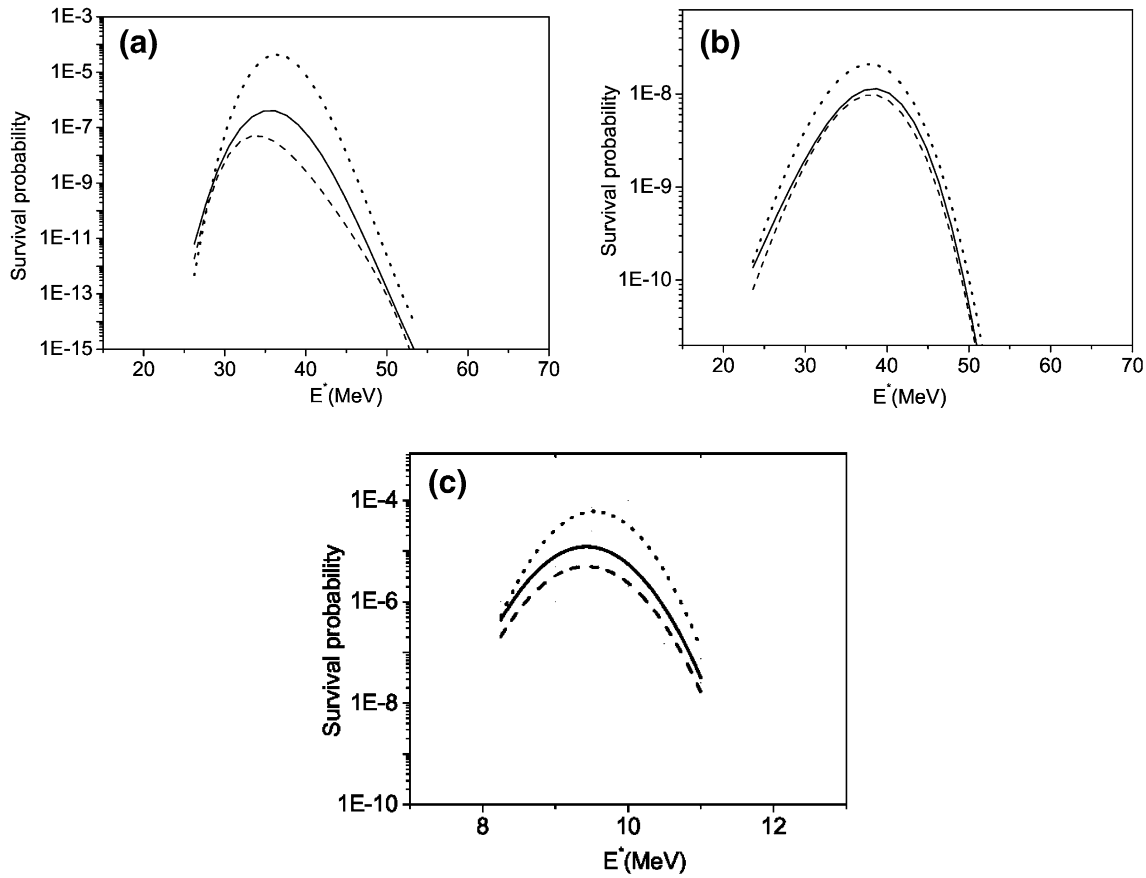

Fig. 3 Plot of survival probability versus energy for **a** $^{48}Ca + ^{238}U$, **b** $^{48}Ca + ^{244}Pu$, **c** $^{70}Zn + ^{208}Pb$ reactions. Dashed, solid, and dotted curves are the results based on three-dimensional Langevin equations without shell effects, four-dimensional Langevin equations without shell effects, and four-dimensional with shell effects, respectively

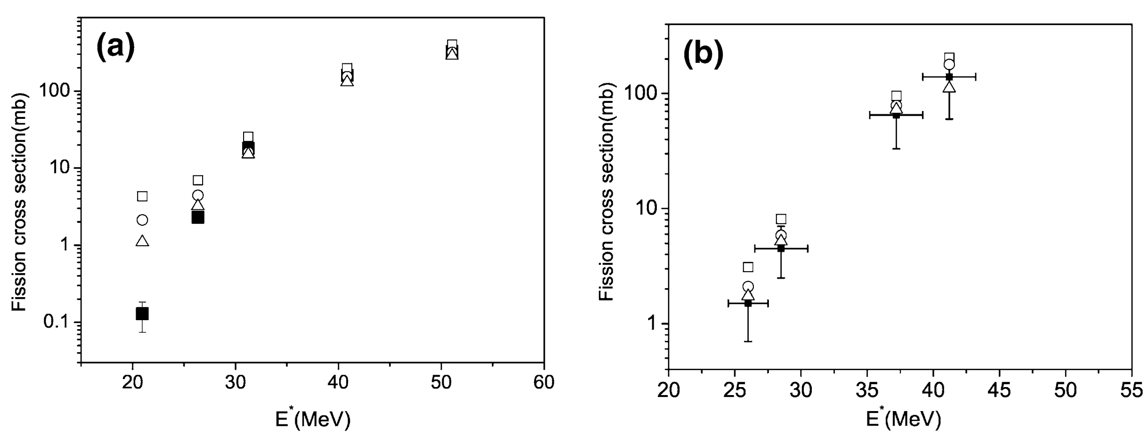

Fig. 4 Variations of fission cross section versus energy for **a** $^{48}Ca + ^{238}U$ reaction, **b** $^{48}Ca + ^{244}Pu$ reaction. Open squares, circles, and triangles show obtained results based on three-dimensional Langevin equations without shell effects, four-dimensional Langevin equations without shell effects, and four-dimensional with shell effects, respectively. Solid squares are experimental data for $^{48}Ca + ^{238}U$ reaction [13] and $^{48}Ca + ^{244}Pu$ reaction [47]

barrier is damped with respect to the angular momentum, l, and nuclear temperature, T, of the compound nucleus. The nuclear temperature is related to the excitation energy, E^*, and the level density parameter, a, by the expression $T = \sqrt{E^*/a}$. The fission barrier was evaluated as [7]

$$B_f(E^*) = B_{LD} - \Delta_{sh} e^{-E^*/E_d}, \tag{15}$$

where B_{LD} is the liquid-drop model fission barrier [43], Δ_{sh} is the shell correction energy calculated for the nucleus in its ground state [44], and $E_{\mathrm{d}} = 18.5$ MeV [45] is the damping parameter which shows a decrease in the shell effects in an energy level density with increasing the excitation energy of the nucleus.

It is worthwhile to note that moreover P_{CN}, the P_{cap} can be calculated by using Langevin equations [46]. However, we have used the approach proposed by Zagrebaev [14], Zagrebaev and Greiner [40].

3 Results

In order to investigate the shell effects and orientation degree of freedom on residue cross section, we selected two hot fusion reactions, ^{48}Ca + ^{238}U and ^{48}Ca + ^{244}Pu with 3n and 4n evaporation channels and three cold fusion reactions, ^{70}Zn + ^{208}Pb, and ^{54}Cr + ^{209}Bi, with 1n and 2n evaporation channels. Also, we performed calculations for 4n and 5n evaporation residue cross section in the ^{26}Mg + ^{238}U reaction. The shell effects were investigated via introducing V_{SH} term in potential energy. The level density parameters of Ref. [35] have been used in calculations. Obtained results are shown in Figs. 1, 2, 3, 4, 5, 6, 7, 8, 9, and 10.

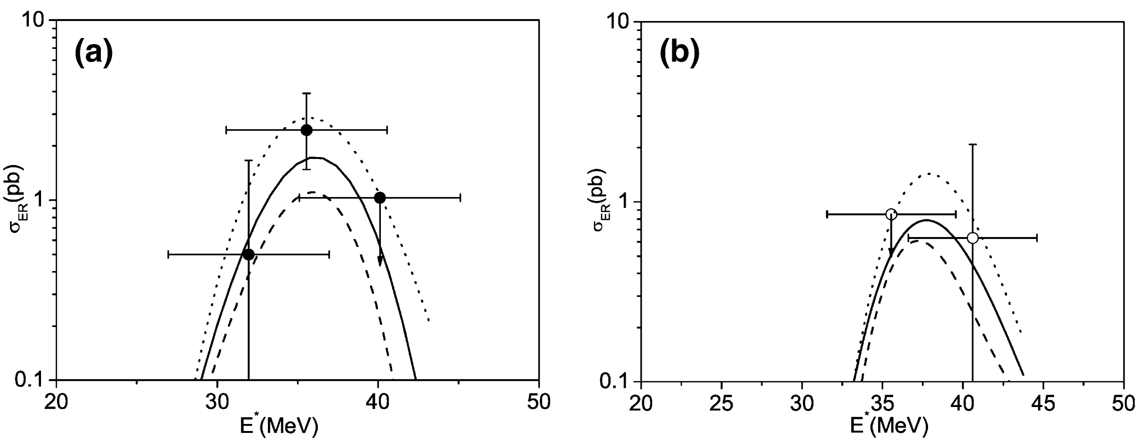

Fig. 5 Plot of excitation functions for **a** 3n and **b** 4n evaporation channels as a function of energy for ^{48}Ca + ^{238}U reaction. Circles are experimental data [47]. Also, dashed, solid, and dotted curves are the results based on three-dimensional Langevin equations without shell effects, four-dimensional Langevin equations without shell effects, and four-dimensional calculations with shell effects, respectively

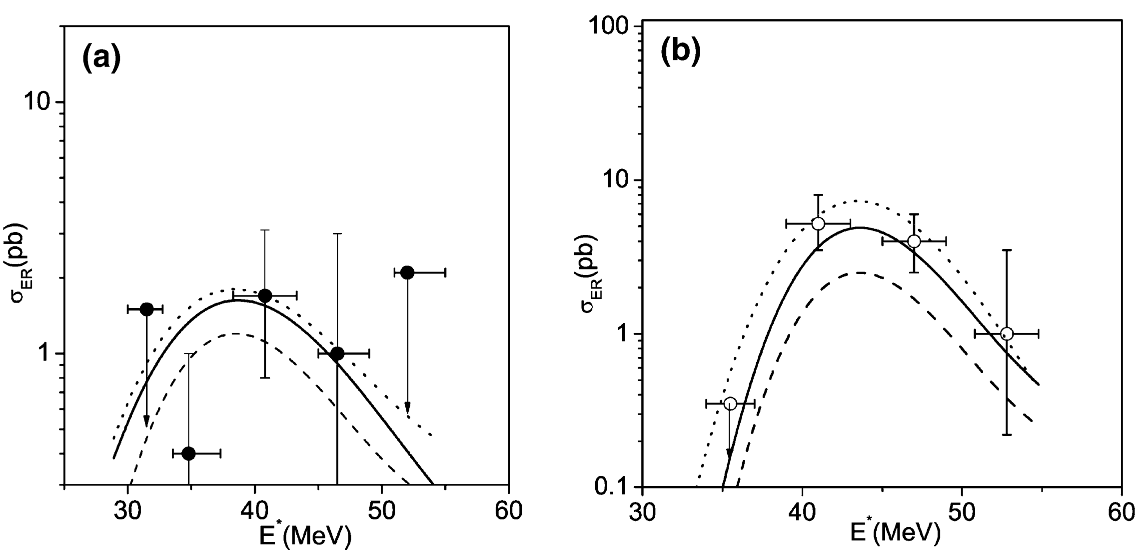

Fig. 6 Same as Fig. 5 for ^{48}Ca + ^{244}Pu reaction

The distribution of the injection distance, $f(s_{inj})$, is calculated with the Langevin equations in three- and four-dimensional collective space. For this reason, we have numerically solved in Eqs. (1) and (9), simultaneously. The injection point distribution is obtained in the simulation with the three- and four-dimensional Langevin equations. One of quantities which changes in three- and four-dimensional calculations is the potential energy. Consequently, the numerical results for the distributions of the injection distance are different in three- and four-dimensional calculations. Obtained results based on the four-dimensional model are higher than results of the three-dimensional model. One can see the discrepancy of two models in Fig. 1, particularly in the position of picks. Figure 1a, b shows variations of the probability distributions of s_{inj} for $^{48}Ca + ^{238}U$ and $^{48}Ca + ^{244}Pu$ reactions, respectively. Dashed, solid, and dotted curves are the results based on three Langevin without shell effects, four-dimensional Langevin without shell effects, and four-dimensional Langevin equations with shell effects, respectively. When s is negative it means that nuclei are crossed. A shape describing the connection of two spheres is depicted in Fig. 1 of Ref. [26]. The probability distributions based on four-dimensional model with shell effects show a noticeable difference and sharper peak in comparison with three- and four-dimensional models without shell effects. For the $^{48}Ca + ^{238}U$ reaction the four-dimensional with shell effects model gives probability distributions larger than three- and four-dimensional models without shell effects particularly around the peak.

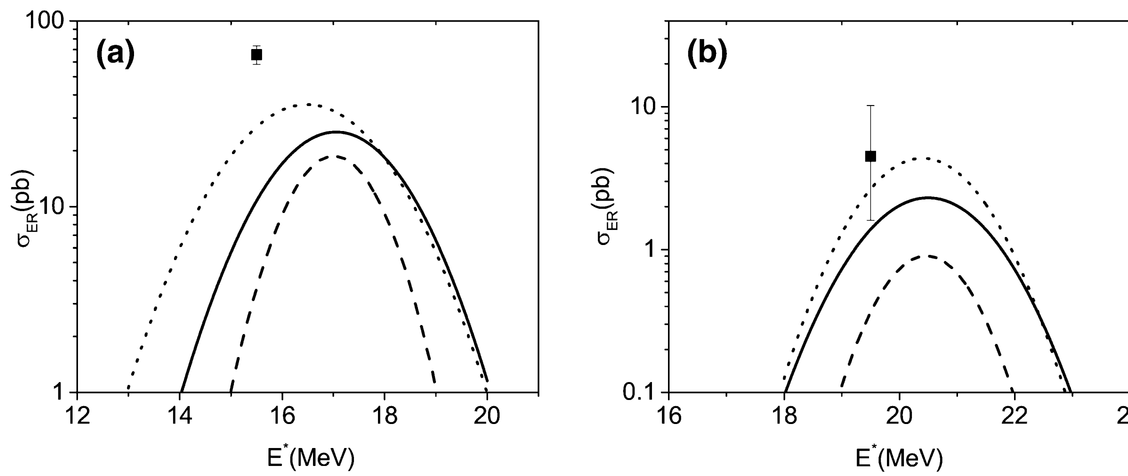

Fig. 7 Variation of excitation functions for **a** $1n$ and **b** $2n$ evaporation channels as a function of excitation energy for $^{58}Fe + ^{208}Pb$ reaction. Squares are experimental data [48]. Also, dashed, solid, and dotted curves are the results based on three-dimensional Langevin equations without shell effects, four-dimensional Langevin equations without shell effects, and four-dimensional with shell effects, respectively

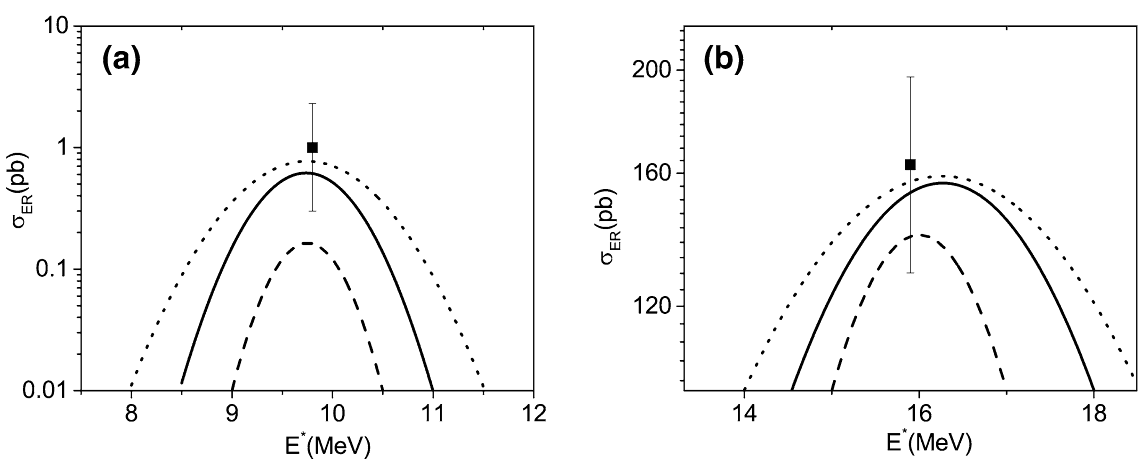

Fig. 8 Variation of excitation functions for $1n$, evaporation channel as a function of excitation energy for **a** $^{70}Zn + ^{208}Pb$ and **b** $^{54}Cr + ^{209}Bi$ reactions. Squares are experimental data [48]. Dashed, solid, and dotted curves are the results based on three-dimensional Langevin equations without shell effects, four-dimensional Langevin equations without shell effects, and four-dimensional with shell effects, respectively

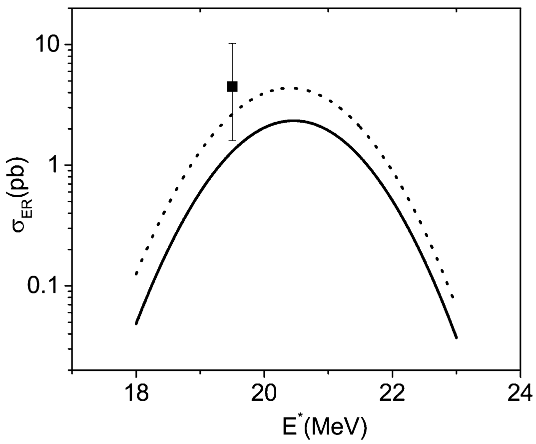

Fig. 9 Variation of excitation functions based on four-dimensional Langevin equations with shell effects for $^{58}Fe + {}^{208}Pb$ reaction in $2n$ evaporation channel as a function of excitation energy for two set of level density parameters. Squares are experimental data [48]. Solid and dotted curves are the calculated excitation functions by using Toke and Swiatecki level density parameter [35] and Ignatyuk parameter [36], respectively

In Fig. 2a, b the plot of the potential energy for $^{48}Ca + {}^{238}U$ and $^{28}Mg + {}^{238}U$ reactions is depicted as a function of elongation. We can see for the case $K \neq 0$ the fission barrier is higher than when comparison with $K = 0$.

The variation of the survival probability as a function of the excitation energy for (a) $^{48}Ca + {}^{238}U$, (b) $^{48}Ca + {}^{244}Pu$, and (c) $^{70}Zn + {}^{208}Pb$ reactions is displayed in Fig. 3. We can observe that by using three- and four-dimensional Langevin equations and with including the shell effects, the peak of the survival probability changes, significantly.

Using Eq. (10), the smooth value of the level density parameter has been modified due to the shell effects. The level density parameter of the daughter nucleus at the ground configuration increases as the excitation energy increases as a result of the damping of the shell correction energy of the ground state. Consequently, the damping of the shell effects directly influences the decay width of neutron emission rather than the fission width.

Figure 4a, b shows variations of fission cross section versus energy for $^{48}Ca + {}^{238}U$ and $^{48}Ca + {}^{244}Pu$ hot fusion reactions, respectively. Open squares, circles, and triangles show obtained results based on three-dimensional Langevin equations without shell effects, four-dimensional Langevin equations with shell effects, and four-dimensional Langevin equations with shell effects, respectively. By increasing the excitation energy, the fission cross section is increased. The obtained results show by increasing the dimension of the Langevin equations the fission cross section is decreased and obtained results based on four-dimensional Langevin equations are in good agreement with the experimental data.

Figures 5 and 6 show the variation of the cross section of evaporation residue as a function of the excitation energy for (a) $3n$ and (b) $4n$ evaporation channels for $^{48}Ca + {}^{238}U$ and $^{48}Ca + {}^{244}Pu$ hot fusion reactions, respectively. The results show by increasing the dimension of the Langevin equations the larger values of evaporation residue cross section are obtained. The obtained results based on four-dimensional Langevin equations with shell effects are in better agreement with the experimental data in comparison with other models. The evaporation residue cross section is related to dimensions of calculations via survival probability.

In Fig. 7a, b the variation of excitation functions for (a) $1n$ and (b) $2n$ evaporation channels as a function of excitation energy is depicted for the $^{58}Fe + {}^{208}Pb$ cold fusion reaction. Similarly, Fig. 8a, b plots the $1n$ evaporation channel for (a) $^{70}Zn + {}^{208}Pb$ and (b) $^{54}Cr + {}^{209}Bi$ cold fusion reactions. Similar results are deduced for these cold fusion reactions. Four-dimensional Langevin equations

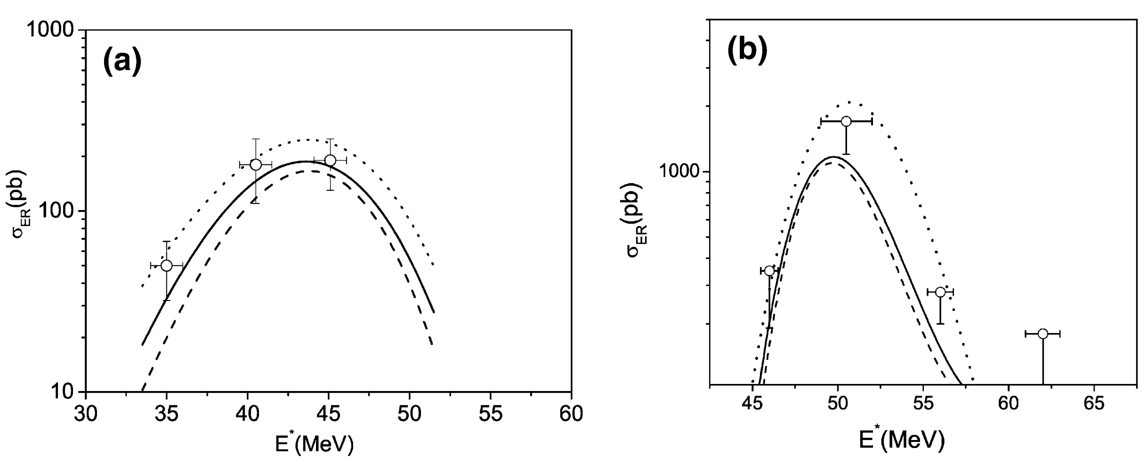

Fig. 10 Plot of excitation functions for $4n$ (**a**) and $5n$ (**b**) evaporation channels as a function of excitation energy for $^{48}Mg + {}^{238}U$ reaction. Circles are experimental data [49]. Also, dashed, solid, and dotted curves are the results based on three-dimensional Langevin equations without shell effects, four-dimensional Langevin equations without shell effects, and four-dimensional with shell effects, respectively

with shell effects are in better agreement with experimental data in comparison with other models, as well.

In order to investigate the effect of the level density parameter on the evaporation residue cross section, the variation of excitation functions for the ^{58}Fe + ^{208}Pb reaction in the 2n evaporation channel based on four-dimensional Langevin equations with shell effects as a function of excitation energy for two set of level density parameters [35, 36] is depicted in Fig. 9. With the decreasing level density parameter the fission cross section decreases, whereas evaporation residue cross section increases. These figures show by using the Ignatyuk parameters, larger values are obtained in comparison with Toke and Swiatecki parameters. For these reactions obtained data by using Ignatyuk parameters are closer to the experimental data, as well.

In Fig. 10 the calculated excitation functions are compared with experimental data (a) 4n and (b) 5n evaporation channels as a function of excitation energy for the ^{48}Ca + ^{238}U reaction. One can see the same results from this figure in comparison with obtained results for ^{48}Ca + ^{244}Pu and ^{48}Ca + ^{238}U reactions. Also, in this figure one can see the shell effects clearly.

Although the calculated results of the evaporation residue cross section in Figs. 5, 6, 7, 8, and 9 agree well with the available experimental results, the limits of this calculation are in the free parameter model dependence in the calculation of capture cross section and in the estimation of the survival probability to fission [50–53].

4 Summary and conclusion

In this paper, the evaporation residue cross sections of two hot fusion reactions, ^{48}Ca + ^{238}U and ^{48}Ca + ^{244}Pu, with 3n and 4n evaporation channels and three cold fusion reactions, ^{70}Zn + ^{208}Pb, and ^{54}Cr +^{209}Bi, with 1n and 2n evaporation channels were calculated by using three- and four-dimensional Langevin equations without shell correction, and four-dimensional Langevin equations with shell correction. Also, the calculations were performed for 4n and 5n evaporation residue cross section in the ^{26}Mg + ^{238}U reaction. The difference between the results of the fission cross section and evaporation residue cross sections based on three- and four-dimensional Langevin equations is significant, and four-dimensional Langevin equations with shell effects give better results in comparison with other models. Our results show that with increasing dimension of Langevin equations the evaporation residue cross section increases, whereas the fission cross section decreases.

References

1. S. Hofmann, G. Münzenberg, The discovery of the heaviest elements. Rev. Mod. Phys. **72**, 733 (2000). https://doi.org/10.1103/RevModPhys.72.733
2. Y.T. Oganessian, F.S. Abdullin, C. Alexander, Experimental studies of the ^{249}Bk + ^{48}Ca reaction including decay properties and excitation function for isotopes of element 117, and discovery of the new isotope ^{277}Mt. Phys. Rev. C **87**, 054621 (2013). https://doi.org/10.1103/PhysRevC.87.054621
3. J.B. Roberto, C.W. Alexander, R.A. Boll et al., Actinide targets for the synthesis of super-heavy elements. Nucl. Phys. A **944**, 99 (2015). https://doi.org/10.1016/j.nuclphysa.2015.06.009
4. X.J. Bao, Y. Gao, J.Q. Li, H.F. Zhang, Influence of nuclear basic data on the calculation of production cross sections of superheavy nuclei. Phys. Rev. C **92**, 014601 (2015). https://doi.org/10.1103/PhysRevC.92.014601
5. X.J. Bao, Y. Gao, J.Q. Li, H.F. Zhang, Isotopic dependence of superheavy nuclear production in hot fusion reactions. Phys. Rev. C **92**, 034612 (2015). https://doi.org/10.1103/PhysRevC.92.034612
6. P. Fröbrich, I.I. Gontchar, Langevin description of fusion, deep-inelastic collisions and heavy-ion-induced fission. Phys. Rep. **292**, 131 (1998). https://doi.org/10.1016/S0370-1573(97)00042-2
7. Z.H. Liu, J.D. Bao, Optimal reaction for synthesis of superheavy element 117. Phys. Rev. C **80**, 034601 (2009). https://doi.org/10.1103/PhysRevC.80.034601
8. D. Naderi, S.A. Alavi, Formation of superheavy elements: study based on dynamical approach. Phys. At. Nucl. **81**, 196 (2018). https://doi.org/10.1134/S1063778818020138
9. N.V. Antonenko, E.A. Cherepanov, A.K. Nasirov et al., Competition between complete fusion and quasi-fission in reactions between massive nuclei. The fusion barrier. Phys. Lett. B **319**, 425 (1993). https://doi.org/10.1016/0370-2693(93)91746-A
10. G.G. Adamian, N.V. Antonenko, S.P. Ivanova et al., Analysis of survival probability of superheavy nuclei. Phys. Rev. C **62**, 064303 (2000). https://doi.org/10.1103/PhysRevC.62.064303
11. A.S. Zubov, G.G. Adamian, N.V. Antonenko, Application of statistical methods for analysis of heavy-ion reactions in the framework of a dinuclear system model. Phys. Part. Nucl. **40**, 847 (2009). https://doi.org/10.1134/S1063779609060057
12. Y. Aritomo, T. Wada, M. Ohta, Y. Abe, Fluctuation-dissipation model for synthesis of superheavy elements. Phys. Rev. C. **59**, 796 (1999). https://doi.org/10.1103/PhysRevC.59.2634
13. K. Nishio, S. Mitsuoka, I. Nishinaka, Fusion probabilities in the reactions ^{40,48}Ca + ^{238}U at energies around the Coulomb barrier. Phys. Rev. C **86**, 034608 (2012). https://doi.org/10.1103/PhysRevC.86.034608
14. V.I. Zagrebaev, Synthesis of superheavy nuclei: nucleon collectivization as a mechanism for compound nucleus formation. Phys. Rev. C **64**, 034606 (2001). https://doi.org/10.1103/PhysRevC.64.034606
15. W.J. Swiatecki, The dynamics of nuclear coalescence or reseparation. Phys. Scr. **24**, 113 (1981). https://doi.org/10.1088/0031-8949/24/1B/007
16. V.L. Litnevsky, V.V. Pashkevich, G.I. Kosenko et al., Description of synthesis of super-heavy elements within the multidimensional stochastic model. Phys. Rev. C **89**, 034626 (2014). https://doi.org/10.1103/PhysRevC.89.034626
17. Z.H. Liu, J.D. Bao, Cold fusion reaction of ^{58}Fe + ^{208}Pb analyzed by a generalized model of fusion by diffusion. Phys. Rev. C **85**, 057603 (2012). https://doi.org/10.1103/PhysRevC.85.057603
18. Z.H. Liu, J.D. Bao, Neutron emission in the fusion process and its effect on the formation of superheavy nuclei. Phys. Rev. C **89**, 024604 (2014). https://doi.org/10.1103/PhysRevC.89.024604

19. Y.J. Liang, M. Zhu, Z.H. Liu et al., Nucleon flow in the process of evolution from dinucleus to mononucleus investigated with a dynamic model. Phys. Rev. C **87**, 047602 (2013). https://doi.org/10.1103/PhysRevC.87.047602
20. G.G. Adamian, N.V. Antonenko, W. Scheid et al., Fusion cross sections for superheavy nuclei in the dinuclear system concept. Nucl. Phys. A **633**, 409 (1998). https://doi.org/10.1016/S0375-9474(98)00124-9
21. J. Hong, G.G. Adamian, N.V. Antonenko, Influence of entrance channel on the production of hassium isotopes. Phys. Rev. C **92**, 014617 (2015). https://doi.org/10.1103/PhysRevC.92.014617
22. L. Zhu, Z.-Q. Feng, C. Li, F.-S. Zhang, Orientation effects on evaporation residue cross sections in ^{48}Ca -induced hot fusion reactions. Phys. Rev. C **90**, 014612 (2014). https://doi.org/10.1103/PhysRevC.90.014612
23. L. Zhu, J. Su, F.S. Zhang, Influence of the neutron numbers of projectile and target on the evaporation residue cross sections in hot fusion reactions. Phys. Rev. C **93**, 064610 (2016). https://doi.org/10.1103/PhysRevC.93.064610
24. D. Naderi, M.R. Pahlavani, S.A. Alavi, Anisotropy of the angular distribution of fission fragments in heavy-ion fusion–fission reactions: the influence of the level-density parameter and the neck thickness. Phys. Rev. C **87**, 054618 (2013). https://doi.org/10.1103/PhysRevC.87.054618
25. Y. Jia, J.D. Bao, Calculations of the anisotropy of the fission fragment angular distribution and neutron emission multiplicities prescission from Langevin dynamics. Phys. Rev. C **75**, 034601 (2007). https://doi.org/10.1103/PhysRevC.75.034601
26. Z.H. Liu, J.D. Bao, Role of the coupling between neck and radial degrees of freedom in evolution from dinucleus to mononucleus. Phys. Rev. C **83**, 044613 (2011). https://doi.org/10.1103/PhysRevC.83.044613
27. J.R. Nix, Further studies in the liquid-drop theory on nuclear fission. Nucl. Phys. A **130**, 241 (1969). https://doi.org/10.1016/0375-9474(69)90730-1
28. K.T.R. Davies, A.J. Sierk, J.R. Nix, Effect of viscosity on the dynamics of fission. Phys. Rev. C **13**, 2385 (1976). https://doi.org/10.1103/PhysRevC.13.2385
29. Y. Aritomo, S. Chiba, Fission process of nuclei at low excitation energies with a Langevin approach. Phys. Rev. C **88**, 044614 (2013). https://doi.org/10.1103/PhysRevC.88.044614
30. S.G. Nilsson, C.F. Tsang, A. Sobiczewski et al., On the nuclear structure and stability of heavy and superheavy elements. Nucl. Phys. A **131**, 1 (1969). https://doi.org/10.1016/0375-9474(69)90809-4
31. F.A. Ivanyuk, S. Chiba, Y. Aritomo, Scission-point configuration within the two-center shell model shape parameterization. Phys. Rev. C **90**, 054607 (2014). https://doi.org/10.1103/PhysRevC.90.054607
32. V.M. Strutinsky, Shell effects in nuclear masses and deformation energies. Nucl. Phys. A **95**, 420 (1967). https://doi.org/10.1016/0375-9474(67)90510-6
33. M.A. Preston, R.K. Bahaduri, *Structure of the Nucleus* (Addison-Wesley publishing Company, Boston, 1975), p. 413
34. T. Asano, T. Wada, M. Ohta et al., Dynamical calculation of multi-modal nuclear fission of fermium nuclei. J. Nucl. Radiochem. Sci. **5**, 1 (2004). https://doi.org/10.14494/jnrs2000.5.1
35. J. Töke, W.J. Światecki, Surface-layer corrections to the level-density formula for a diffuse Fermi gas. Nucl. Phys. A **372**, 141 (1981). https://doi.org/10.1016/0375-9474(81)90092-0
36. A.V. Ignatyuk, Contribution of collective motions to density of excited-states of a nucleus. Yad. Fiz. **21**, 1185 (1975). [Sov. J. Nucl. Phys. 21, 612 (1975)]
37. M. Brack, J. Damgaard, A.S. Jensen, Funny hills: the shell-correction approach to nuclear shell effects and its applications to the fission process. Rev. Mod. Phys. **44**, 320 (1972). https://doi.org/10.1103/RevModPhys.44.320
38. P.N. Nadtochy, E.G. Ryabov, A.E. Gegechkori et al., Four-dimensional Langevin dynamics of heavy-ion-induced fission. Phys. Rev. C **85**, 064619 (2012). https://doi.org/10.1103/PhysRevC.85.064619
39. D. Naderi, A dynamical interpretation of fusion fission reactions using four-dimensional Langevin equations. J. Phys. G Nucl. Part. Phys. **40**, 125103 (2013). https://doi.org/10.1088/0954-3899/40/12/125103
40. V.I. Zagrebaev, W. Greiner, Cross sections for the production of superheavy nuclei. Nucl. Phys. A **944**, 257 (2015). https://doi.org/10.1016/j.nuclphysa.2015.02.010
41. W.J. Swiatecki, K. Siwek-Wilczynska, J. Wilczynski, Fusion by diffusion. Acta Phys. Pol. B **34**, 2049 (2003)
42. Z. Min, F. Jun-Li, Q. Zhen, The Role of neck evolution in the synthesis of superheavy element 112. Chin. Phys. Lett. **30**, 082401 (2013). https://doi.org/10.1088/0256-307X/30/8/082401
43. A.J. Sierk, Macroscopic model of rotating nuclei. Phys. Rev. C **33**, 2039 (1986). https://doi.org/10.1103/PhysRevC.33.2039
44. P. Möller, J.R. Nix, W.D. Myers et al., Nuclear ground-state masses and deformations. At. Data Nucl. Data Tables **59**, 185 (1995). https://doi.org/10.1006/adnd.1995.1002
45. K. Siwek-Wilczyńska, I. Skwira, J. Wilczyński, Tests of the fission-evaporation competition in the deexcitation of heavy nuclei. Phys. Rev. C **72**, 034605 (2005). https://doi.org/10.1103/PhysRevC.72.034605
46. Z. Liu, J.D. Bao, Systematical calculations of the ^{136}Xe(^{136}Xe, xn)$^{272-x}$Hs reaction: Effects of quasifission in the early stage of the fusion process. Phys. Rev. C **81**, 044606 (2010). https://doi.org/10.1103/PhysRevC.81.044606
47. Y.T. Oganessian, V.K. Utyonkov, Y.V. Lobanov, Measurements of cross sections and decay properties of the isotopes of elements 112, 114, and 116 produced in the fusion reactions ^{233,238}U, ^{242}Pu, and ^{248}Cm + ^{48}Ca. Phys. Rev. C **70**, 064609 (2004). https://doi.org/10.1103/PhysRevC.70.064609
48. G.G. Adamian, N.V. Antonenko, W. Scheid, Isotopic dependence of fusion cross sections in reactions with heavy nuclei. Nucl. Phys. A **678**, 24 (2000). https://doi.org/10.1016/S0375-9474(00)00317-1
49. J.M. Gates, M.A. Garcia, K.E. Gregorich, Synthesis of rutherfordium isotopes in the ^{238}U(^{26}Mg, xn)$^{264-x}$Rf, reaction and study of their decay properties. Phys. Rev. C **77**, 034603 (2008). https://doi.org/10.1103/PhysRevC.77.034603
50. W. Loveland, An experimentalist's view of the uncertainties in understanding heavy element synthesis. Eur. Phys. J. A **51**, 120 (2015). https://doi.org/10.1140/epja/i2015-15120-2
51. X.J. Bao, S.Q. Guo, H.F. Zhang, Influence of proton shell closure on the evaporation residue cross sections of superheavy nuclei. J. Phys. G Nucl. Part. Phys. **44**, 045105 (2017). https://doi.org/10.1088/1361-6471/aa53e8
52. G. Giardina, G. Mandaglio, A.K. Nasirov et al., Uncertainties and understanding of experimental and theoretical results regarding reactions forming heavy and superheavy nuclei. Nucl. Phys. A **970**, 169 (2018). https://doi.org/10.1016/j.nuclphysa.2017.11.010
53. X.J. Bao, S.Q. Guo, H.F. Zhang et al., Dynamics of complete and incomplete fusion in heavy ion collisions. Phys. Rev. C **97**, 024617 (2018). https://doi.org/10.1103/PhysRevC.97.024617